Lake Erie hypoxia spatial and temporal dynamics present challenges for assessing progress toward water quality goals

Craig A. Stow[a*], Mark D. Rowe[a], Casey M. Godwin[b], Lacey A. Mason[a], Peter J. Alsip[b], Richard T. Kraus[c], Thomas H. Johengen[d], and Stephen A. Constant[a]

[a]National Oceanic and Atmospheric Administration, Great Lakes Environmental Research Laboratory, Ann Arbor, MI

[b]Cooperative Institute for Great Lakes Research, University of Michigan, Ann Arbor, MI

[c]United States Geological Survey, Great Lakes Science Center, Lake Erie Biological Station, Huron, OH

[d]Michigan Sea Grant, University of Michigan, Ann Arbor, MI

*craig.stow@noaa.gov

Orcids: Rowe (0000-0002-0852-3346), Mason (0000-0003-1541-3134), Godwin (0000-0002-4454-7521), Stow (0000-0001-6171-7855), Kraus (0000-0003-4494-1841), Alsip (0000-0002-9830-914X)

Abstract

Seasonal hypolimnetic hypoxia has been documented in Lake Erie's central basin since the 1950s. Ship-based surveys to monitor hypoxia have been conducted since the 1980s, but they occur at a relatively low frequency and focus on the deeper areas of the central basin. To better document the seasonal development of stratification and the consequent occurrence of hypoxia, we deployed eight moorings, in both nearshore-shallow areas and offshore-deep areas of the central basin, equipped with temperature and oxygen sensors at multiple depths, that recorded temperature and oxygen concentrations every 10 minutes. Results from 2017-2019 reveal that hypoxia occurs as early as July in the shallower areas west of, and around the southern perimeter of the central basin, but does not occur until August or September in the deeper central basin. Hypoxia is intermittent in the shallower perimeter areas; whereas in the deeper areas, hypoxia can persist into October, often progressing to anoxia. The intra and interannual differences in the spatial and temporal extent of hypoxia indicate that an extensive monitoring program will be necessary to more accurately assess progress toward reducing the extent of hypoxia pursuant to the lake ecosystem objectives of the 2012 Great Lakes Water Quality Agreement.

Keywords: seasonal hypolimnetic hypoxia, eutrophication, oxygen depletion, stratification, Great Lakes Water Quality Agreement, phosphorus load targets, lake ecosystem objectives

Introduction

Seasonal hypolimnetic hypoxia (dissolved oxygen < 2 mg/L) is well-documented in aquatic ecosystems worldwide (Diaz 2001, Jenny et al 2016, Jane et al 2021). In lakes hypoxia typically occurs when temperature-induced stratification prevents oxygenated surface water from mixing throughout the water column, allowing settled organic matter degradation to deplete dissolved oxygen (DO) below the thermocline. Often hypoxia is a symptom of eutrophication (Carpenter et al. 1998), as excessive primary production caused by high nutrient inputs produces decaying organic matter that accumulates in the profundal zone. Depending on the hypoxia duration and concentration to which DO is depleted, changes in water chemistry and habitat quality may ensue.

Hypoxia is a long-standing phenomenon in Lake Erie (Figure 1). Early documentation occurred in 1953 (Britt 1955) in Lake Erie's western basin, although this basin is relatively shallow (<10 m) and experiences limited stratification. While oxygen depletion has been periodically reported in the western basin since then (Carr et al 1965, Britt 1968, Jabbari et al 2019), the main area of concern is the central basin, which is sufficiently deep (>20m) to experience persistent summer stratification. Paleolimnological evidence suggests periodic central basin hypoxia may have occurred for thousands of years (Delorme 1982). However, while surveys in 1929 (Fish 1960) and from 1947-53 (Powers et al 1959, 1960) revealed hypolimnetic water below DO saturation, hypoxia was not directly observed until the late 1950s (Beeton 1961, Carr 1962, Beeton 1965) and has been seen in routine surveys since then (Scavia et al 2014), encompassing an estimated seasonally averaged areal extent of up to ~8.8 x 10^3 km^2 (Zhou et al 2015). Central basin hypoxia is driven by deposition of organic matter produced in the photic zone (Burns and Ross 1972 Project Hypo report), though the importance of organic matter from the highly productive western basin versus the central basin remains uncertain (Watson et al 2016, Reavie et al 2016). The spatial extent and duration of hypoxia can vary annually depending on weather and nutrient inputs (Rowe et al., 2019; Bocaniov et al 2020). Documented effects of central basin hypoxia include accelerated sediment phosphorus release (Anderson et al 2021a), modified fishery habitat (Vanderploeg et al 2009, Kraus et al 2015), and water quality impairment at drinking water intakes (Ruberg et al 2008).

The Great Lakes Water Quality Agreement (GLWQA), originally signed in 1972, is a compact between Canada and the United States to reduce water pollution and related problems throughout the Laurentian Great Lakes. To reduce eutrophication symptoms, the GLWQA included total phosphorus load targets for each lake, including an 11,000 metric ton/year goal for Lake Erie. Management actions taken to meet these targets were initially successful (DePinto et al 1986); by the 1990s Lake Erie was considered to have largely recovered (Makarewizc and Bertram 1991, Makarewicz and Bertram 1993), and retrospective analyses suggest that central basin hypoxia diminished during that time (Burns et al 2005, Zhou et al 2013). However, by the early 2000s hints of "re-eutrophication" became apparent, including a massive algal bloom in 2011 (Michalak et al. 2013).

To address re-eutrophication and other emerging concerns, the GLWQA was updated in 2012 and included the following "lake ecosystem objective" to reduce central basin hypoxia: "minimize the extent of hypoxic zones in the Waters of the Great Lakes associated with excessive phosphorus loading, with particular emphasis on Lake Erie", as well as a charge to reevaluate the 1978 total phosphorus load targets (Great Lakes Water Quality Agreement 2012). In response, new objectives aimed at reducing hypoxia were adopted in 2016, which included a 6,000 metric ton/year total phosphorus load target for inputs upstream of the central basin, and a goal of achieving an average DO concentration of > 2 mg/L from August to September in the central basin hypolimnion (Annex 4 Objectives and Targets Task Team Final Report to the Nutrients Annex Subcommittee 2015). Management activities are currently underway throughout the Lake Erie drainage basin to reduce phosphorus inputs, and an Adaptive Management strategy is in development (Stow et al 2020) to evaluate progress toward meeting the updated phosphorus targets (Rowland et al 2021) and document improvements in the lake.

Tracking and reporting the response of Lake Erie under an adaptive management program requires accurate measurement of when and where hypoxia occurs so that it can be quantified with appropriate metrics to assess progress toward meeting established goals. Recent analyses of hypoxia in the central basin have relied on data from long-term monitoring sites that are located in the deeper area of the basin (> 20 m) and visited one or two times per month in August and September (Zhou et al 2013; Scavia et al 2014). Because the hypolimnion is relatively thin in shallower stratified areas (10-20 m), oxygen depletion takes less time than in deeper areas (> 20 m) where the hypolimnion is thicker. Thus, in contrast with the conventional wisdom, modeling results indicate that hypoxia tends to progress from the nearshore to the offshore (Rowe et al. 2019). While those offshore sites have the longest consistent record, the locations may not reflect patterns that occur in shallower areas around the periphery of the basin and the measurement frequency is unlikely to capture short-term and early-season (July) events (Ruberg 2008). Thus, more detailed observations are required to assess predictive models of features such as hypoxic upwelling events, which occur regularly at the margins of the hypolimnion (Rowe et al.2019).

We describe initial observations from a mooring network of moorings deployed throughout the basin to continuously measure DO and thermal structure during the hypoxia season, including nearshore locations along the Ohio shoreline. These observations offer an improved understanding of hypoxia dynamics in Lake Erie, and will promote future model upgrades, as well as better assessments of the response of hypoxia to changing nutrient inputs.

Methods

We deployed moorings at eight sites (SI Table 1) around Lake Erie's central basin (Figure 1) from approximately May-September in 2017-2019. The sites were chosen to support development of a hypoxia forecast model to provide an early warning to drinking water managers along the Ohio coast so that they could prepare to adjust water treatment methods when it was likely that hypoxic water would be drawn into their intakes (Rowe et al 2019). Each mooring had sensors at multiple depths throughout the water column that logged temperature and DO at 10-minute intervals. The number of sensors on each mooring differed somewhat each year depending on water depth and expectations regarding the depth and thickness of the thermocline (SI Table 2). Generally, there were more temperature than DO sensors on each mooring.

We recorded temperature using SeaBird Scientific SBE 56 sensors and RBR Ltd Solo sensors; the accuracy and specifications of these sensors was identical (±0.002°C). Dissolved oxygen was measured using Precision Measurement Engineering MiniDot Loggers (+/- 5% of the measurement or +/- 0.3 mg/l, whichever is larger) that included wipers to ensure biofouling was minimized. The DO sensors included internal temperature sensors for calculating DO, which we determined to be as accurate as the SBE56 and RBR Solo temperature loggers. We attached multi-parameter sondes (YSI EXO) around 2 m in depth to moorings 2 and 9 that measured DO (accuracy of ±0.1 mg/L or 1% of reading) and temperature (±0.01°C). We outfitted every mooring with two U20L-02 pressure sensors from Onset, Inc, to determine vertical movement of the sensor line in the water column during deployment.

The mooring design was a "U" shape (SI Figure 1) to allow attachment of multiple sensors below a surface spar buoy (Rolyan B961R). The sensors were secured via PVC clamps to the ¼" stainless steel 7 x 16 wound aircraft cable, which was attached to 15ft. of ½" long link chain anchored to a 68 kg concrete weight. There was a ~100 m groundline (1/2" MFP Floatline, Samson Ropes) taped at meter intervals to a ¼" stainless steel cable as a tensioner to another 68 kg concrete weight. The rest of the sensors were floated above this weight using a sub-surface float with 18 kg buoyancy. This design facilitated multiple ways of mooring recovery, while dampening wave action due to the chain and isolating the bottom-most sensors to prevent wave action damage.

Following mooring retrieval each year we downloaded and examined the temperature and DO data to discover any sensor failures or other obvious anomalies in the data. The curated data were archived and are available at NOAA National Centers for Environmental Information (https://doi.org/10.25921/qd27-bj97). Because ship traffic limited our ability to attach sensors to measure water surface conditions we used satellite-measurements for surface temperature and estimated surface DO as the freshwater saturation value corresponding to the satellite surface temperature (Great Lakes Surface Environmental Analysis [GLSEA]; https://coastwatch.glerl.noaa.gov/).

We defined hypoxia as DO < 2 mg/L and anoxia as DO < 0.15 mg/L (the highest recorded concentration when the sensors were placed in water made anoxic by potassium metabisulfite addition). To assess the strength of stratification we calculated the potential energy anomaly (PEA), a measure of the energy required ($J\ m^{-3}$) to fully mix the water column (Simpson and Bowers 1981). PEA is a local measure that is similar to Schmidt stability, which was developed to indicate water column stability at the whole lake-scale (Schmidt 1928).

PEA is defined as:

$$\varphi = \frac{1}{h}\int_{-h}^{\eta} (\bar{\rho} - \rho) g z \mathrm{d}z$$

where ρ = the vertical density profile over the water column depth, h, η = the water surface, $\bar{\rho}$= the depth averaged density, z = the vertical coordinate, and g = the gravitational acceleration. In freshwater, an isothermal water column has a PEA of zero; higher values indicate increasing stratification; a PEA of 10 J m^{-3} has been used to indicate stratification in coastal marine systems (Simpson et al 1977; Simpson and Bowers 1984). Operationally, we use a PEA of < 2 J m^{-3} to indicate no stratification, a PEA ≥ 2 and < 10 J m^{-3} to indicate light stratification, a PEA ≥ 10 and < 20 J m^{-3} to indicate stratification, and a PEA ≥ 20 to indicate strong stratification.

Our main presentation includes plots of temperature and DO vs. time, linearly interpolated with depth, for each site for all three years (Figures 2 and 3). We included time-series plots from every sensor, labeled to correspond to the interpolated plots, in the supplemental information (SI Figures 2 and 3) to view features difficult to discern in the interpolated plots.

Results

We organized the results by both depth and location within the basin.

Shallow (<20 m), nearshore sites along central basin southern perimeter (Sites 1, 3, 5, and 8)

Site 1

We obtained high-resolution temperature data through the water column in 2017 and 2019 (Figure 2 a,c) as well as near-surface and bottom DO data (Figure 2 m,o). In 2018 surface sensors were lost; only bottom temperature and DO data were available (Figure 2 b,n).

Weak vertical temperature gradients were apparent by late May every year, followed by light stratification through June, intermittent stratification in July and intermittent light stratification though September (Figure 2 a-c, m-o; Figure 4). When stratification occurred, the hypolimnion thickness was generally < 3 m.

Periodic hypoxia was evident by mid-July, with the earliest occurrence in 2019 on July 4 (Figure 4). The number of hypoxic days ranged from approximately 21 in 2017 to 40 in 2019; we note that in 2017 bottom DO had just dipped below 2 mg/L when mooring was retrieved (Figure 2 m). In addition to hypoxia, Site 1 also experienced periods of anoxia each year (Figure 4); often these occurred as repeated events of short duration when the water column was only weakly stratified (Table 1, Figure 4). Every year there were periods when the lowest DO was not at the bottom, particularly in early September, a possible indication of benthic primary production (SI Figure 2 m,n,o).

Site 3

High-resolution, surface-to-bottom temperature data were available every year (Figure 2 d,e,f) as were near-surface and near-bottom DO measurements; therefore resolution on the interpolated DO plots is limited across the intermediate depths (Figure 2 p,q,r).

Light stratification was apparent in late May every year (Figure 2 d,e,f; Figure 4) accompanied by slight DO depletion near the bottom (Figure 2 p, q, r). While a brief hypoxic episode occurred in late June 2017, hypoxia did not usually occur until early July, even though stratification was occurring in June (Figure 4). Stratification strength varied and hypoxia was intermittent throughout deployment in all three years; the number of hypoxic days ranged from 39 in 2017 to 51 in 2019 (Table 1); in 2017 the DO was dropping rapidly at the time the mooring was retrieved and hypoxia may have reoccurred after removal. Intermittent anoxia also occurred, ranging from 7 anoxic days in 2017 to 27 in 2019 (Table 1).

Site 5

High-resolution, surface-to-bottom temperature data were recorded in 2017 and 2019 (Figure 2 g, i). DO data were recorded at three near-bottom depths in 2017 and 2019, and at the one meter depth in 2019 (Figure 2 s, u). No mid-depth DO data were recorded in either year. In 2018, the mooring became detached during a storm and, though it was recovered, contained no salvageable data.

Light stratification occurred by late May in both 2017 and 2019 (Figure 2 g, i; Figure 4) accompanied by rapid DO depletion near the bottom, though hypoxia did not occur until mid-July in 2017 and early August in 2019 (Figure 2 s, u; Figure 4). In 2017, the water column had become nearly isothermal by the end of June and bottom DO had returned to near saturation (Figure 2 g, s; Figure 4). From July-August 2017 stratification strength varied, with the hypolimnion thickness ranging from ~ 1.5 to 9 m, accompanied by rapid DO depletion and hypoxia (Figure 2 s; Figure 4).

In contrast to 2017, stratification was stronger and more persistent in 2019, with a progressive deepening of the thermocline into early August and intermittent stratification near the bottom into mid-September (Figure 2 i; Figure 4). DO depletion occurred through July, however hypoxia did not begin until early August and was nearly continuous into late September (Figure 2 u; Figure 4). Although the patterns over the season differed, Site 5 experienced 40 hypoxic days in both 2017 and 2019 (Table 1). Periods of anoxia also occurred with 12 anoxic days in 2017 and 23 in 2019.

Site 8

We obtained medium-high-resolution temperature data throughout water column each year (Figure 2 j, k, l) and near-surface and bottom DO data (Figure 2 v, w, x).

Site 8 was lightly stratified by late May every year, with extended, intermittent, strong stratification from July-August in 2018 and 2019 (Figure 2 j, k, l; Figure 4). Although DO depletion usually accompanied stratification, hypoxia was rare, occurring at an intermediate depth (11 m) in 2018 while the bottom sensor did not report hypoxia (SI Figure 2 w). During 2019, Site 8 experienced two brief hypoxic periods at the bottom sensor, but only one of those lasted longer than 24 hours (SI Figure 2 x; Figure 4). DO was periodically higher at the bottom than several meters off the bottom, possible evidence of benthic primary production (SI Figure v, w, x). The number of hypoxic days at Site 8 was the least of all the moorings, with only 2 days recorded in 2019 (Table 1). No anoxia was detected at this site (Table 1).

Deeper, offshore sites (Sites 2, 4, 7, and 9)

Site 2

In 2017 we obtained temperature and DO data only at mid-depths; in particular no bottom DO data were obtained in 2017 limiting our assessment of hypoxia and anoxia (Table 1, Figure 4). In 2018 we obtained temperature and DO measurements near the surface until September and at mid-bottom depths for the duration of deployment, and in 2019 high-resolution temperature data spanning the water column were available for most of the season (Figure 3 a, b, c, m, n, o).

Stratification was established by the time of deployment in early June in 2017 and 2018; an earlier deployment in 2019 revealed stratification had developed in late May (Figure 3 a, b, c; Figure 4). By July each year strong stratification was well-established with a hypolimnion thickness of ~ 4 m. Every year the thermocline became deeper by late July with a hypolimnion thickness of < 3 m by August. Based on the bottom-most sensor, hypoxia was intermittent in

July every year; in 2017 the apparent absence of hypoxia for most of August may have been an artifact of not having a bottom sensor (Figure 3 m). In 2018 and 2019 hypoxia was present through most of August and much of September, (Figure 3 n, o; Figure 4) though the number of hypoxic days was much greater in 2019 than 2018, 67 vs. 37 (Table 1). There were periods every year (July and August 2018, briefly in July 2019) when the bottom DO was greater than some other sensors higher in the water column, a possible indication of benthic primary production (SI Figure 3 m, n, o). Anoxia was also recorded at Site 2 with an extended period from late July into October in 2019 (Figure 3 o; Figure 4)

Site 4

Site 4 was in the deepest region of the central basin. Due to its proximity to shipping lanes this mooring had no surface expression; the top sensors were at 8 m depth. Additionally, the location differed slightly after 2017 to avoid conflicts with vessel traffic (Figure 1). High-resolution temperature data were available every year from 8 m depth to bottom (Figure 3 d, e, f), DO sensors extended over the same depth range, but with lower resolution (Figure 3 p, q, r).

Light stratification was established by deployment in late May each year, with stratification to strong stratification occurring by mid-June (Figure 3 d, e, f; Figure 4). Generally, the thermocline became progressively deeper from July into August though the pattern and timing differed every year. Hypolimnion thickness was approximately 9 m in early July, but decreased to 2-4 m by August. In all three years, prior to the onset of hypoxia, there were periods when the DO near the bottom exceeded the DO at shallower depths (SI Figure 3 p, q, r); this phenomenon was particularly pronounced from mid-July – mid-August in 2019 (SI Figure 3 r). Site 4 became hypoxic later than the shallower sites and Site 2; the earliest onset of hypoxia was in 2017 on August 1, the latest in 2018 on September 9 (Figure 4, Table 1). In contrast to the shallower, nearshore locations, once hypoxia was established it was generally sustained and progressed to anoxia. In 2017 and 2018 anoxia occurred until the moorings were removed; in 2019 mooring retrieval was somewhat later revealing anoxia persisted into October, ending just before the mooring was retrieved on October 10. At the time the moorings were retrieved the number of hypoxic days, up to that time, ranged from 26 in 2018 to 55 in 2017 (Table 1). The number of anoxic days, up until mooring retrieval, ranged from 23 in 2018 to 37 in 2017 (Table 1).

Site 7

The available measurements differed each year; in 2017 we obtained medium-resolution temperature and DO data from 8-19.6 m, in 2018 high-resolution temperature data were available from 1-19.6 m and medium-resolution DO data were available from 1-17.1 m as the bottom DO sensor was faulty. We obtained high resolution temperature data from 2-16 m in 2019 (Figure 3 g, h, i) with near-surface DO data (1 m) and medium-resolution data from 8-14.1 m; no bottom DO data were collected in 2019 (Figure 3 s, t, u).

Stratification occurred by mid-June and was often strong into late August - early September (Figure 3 g, h, i; Figure 4) every year. The thermocline depth varied over periods of days-weeks and was generally deepest in July; becoming shallower through August when the hypolimnion sometimes exceeded a 10 m thickness. Though the absence of bottom DO data in 2018 and 2019 limits our ability to make strong inference, the available information suggests that there was a steady, progressive DO decline from early June into August each year while hypoxia became established by early-late August and became intermittent by early September (Figure 3 s, t, u; Figure 4). In 2017 we recorded 31 hypoxic days and 14 anoxic days, although anoxia was still present when the mooring was retrieved (Figure 3 s; Figure 4). Because there were no bottom DO sensors in 2018 and 2019 the number of hypoxic days could not be reliably estimated, however the deepest sensor indicated at least 18 days in 2018 at 17.1 m and 9 days at 14.1 m in 2019.

Site 9

In 2017 and 2018 we obtained near-surface temperature data (the surface sensor malfunctioned in late August 2017) and medium-resolution temperature data near the bottom (Figure 3 j, k). In 2019 high-resolution temperature data were available from near-surface to bottom (Figure 3 l). The available DO data were similar every year, with medium-resolution data from mid-depth to bottom (Figure 3 v, w, x).

Light stratification was established by late May in 2017 and 2019, and stratification was already occurring when the mooring was deployed on May 23rd in 2018 (Figure 3 j, k, l; Figure 4). In 2017, the thermocline was about 17 m deep by early July with a hypolimnion thickness of approximately 2 m. In 2018 and 2019, the thermocline was only about 10 m deep by early July and became progressively deeper into August. In 2017, hypoxia was apparent by early August but not until early September in 2018 and 2019 (Figure 3 v, w, x; Figure 4). The number of hypoxic days ranged from 30 in 2017 to 33 in 2019, although hypoxia was still occurring when the mooring was retrieved in late September in 2017 and early October in 2019 (Table 1; Figure 4). Periodic anoxia was also present ranging from least 8 anoxic days in 2017 to 20 in 2019.

Weather events

Regional weather events strongly influenced stratification and DO dynamics across sites in all three years. All sites experienced a nearly-simultaneous pre-destratification cooling event in late August- early September each year (SI Table 3, SI Figure 4), associated with air temperature becoming cooler than surface water temperature, and increased wind speed in some years. This cool air, and in some cases increased wind, mixed and cooled the surface water, *usually* deepening the thermocline.

In 2017, this cooling was followed by an unusually warm period from September 16-27. In Cleveland, OH the air temperature peaked at 34.4 ºC on September 25, approximately 7.6 ºC above average (https://www.weather.gov/wrh/Climate?wfo=cle). This warm period induced an approximately 3ºC temperature gradient over the top 10-15 m of water at most sites, accompanied by rapid oxygen depletion at the bottom.

Shallow, nearshore sites

At Site 1, the shallowest mooring, the annual cooling events resulted in nearly isothermal conditions (Figure 2 a, b, c) and the cessation of hypoxia (Figure 2 m, n, o). However, the mid-September 2017 warm, calm period produced a temperature gradient (Figure 2 a) sufficient to cause DO depletion at the bottom, which was approaching hypoxia at the time the mooring was retrieved in late September (SI Figure 2 m).

At Site 3 the temperature dynamics following the cooling event differed among years; in 2017 and 2018 surface to bottom mixing resulted with nearly isothermal conditions and a cessation of hypoxia followed (Figure 2 d, e; Figure 2 p, q) while in 2019 both stratification and hypoxia persisted (Figure 2 f; Figure 2 r). The September 2017 warm, calm period caused restratification accompanied by rapid DO depletion at the bottom, however conditions had not become hypoxic by the time the mooring was removed (Figure 2 d; Figure 2 p).

Site 5 exhibited dynamics similar to Site 1 in 2017, the cooling event produced nearly isothermal conditions (Figure 2 g) with a cessation of hypoxia (Figure 2 s) and the subsequent warm period corresponded to reestablishment of a temperature gradient accompanied by rapid hypolimnetic DO depletion and a brief period of hypoxia. While no Site 5 data were available for

2018, in 2019 dynamics following the cooling event were similar to those at Site 3 with the persistence of both stratification and hypoxia (Figure 2 i; Figure 2 u).

Site 8 temperature dynamics were similar to Sites 3, and 5 with nearly isothermal conditions following the cooling events in 2017 and 2018 and intermittent stratification persisting in 2019 (Figure 2 j, k, l). While hypoxia was never recorded in 2017 at this site, bottom DO dropped quickly during the September restratification, reaching a concentration of approximately 2.2 mg/L, the lowest bottom DO conditions recorded that year, just before the mooring was removed (SI Figure 2 v).

Deeper, offshore sites

The late August-early September cooling event (SI Table 3) was also evident at Site 2. While temperature and oxygen dynamics in 2017 were unclear due to the lack of both surface and bottom sensors (Figure 3a) the responses differed in 2018 vs. 2019. In 2018 complete surface to bottom mixing resulted in isothermal conditions (Figure 3b), while only a slight deepening of the thermocline occurred in 2019 (Figure 3 c). Despite essentially isothermal conditions a brief reoccurrence of hypolimnetic hypoxia occurred in 2018 (Figure 3 n) while in 2019 hypoxia persisted until the mooring was removed (Figure 3 o).

At Site 4, stratification persisted following the cooling events; in 2017 and 2018 the thermocline actually became shallower following the events (Figure 3 d, e), while in 2019 it became slightly deeper (Figure 3 f). In 2017 and 2019 hypoxia and anoxia persisted following the cooling (Figure 3 p, r); in 2018 the *onset* of hypoxia was approximately concurrent with the sudden cooling (Figure 3 q; Figure 4). The 2017 warm, calm period induced a temperature gradient in approximately the top 11 m of water (Figure 3 d), however because there was still a pronounced thermocline at approximately 20 m there was no obvious effect on hypolimnion DO, which remained anoxic (Figure 3 p).

While Site 7 also experienced these cooling events every year, the absence of a surface temperature sensor in 2017 (Figure 3 g) and bottom DO sensors in 2018 and 2019 (Figure 3 t, u) make the changes upon cooling less clear than at other sites. However, there were periods of hypolimnetic DO depletion following these events in all three years (Figure 3 s, t, u) and hypoxia reoccurred in 2017, associated with the late September warming. Additionally, a brief hypoxic period was recorded in 2019 at the 11.1 m sensor, approximately 5 m off the bottom.

Dynamics at Site 9 differed every year following the cooling event. In 2017 it quickly became isothermal (Figure 3 j), in 2018 the thermocline became shallower (Figure 3 k), and in 2019 the thermocline became deeper (Figure 3 l). In 2017, following a several day isothermal period and the cessation of hypoxia, the water restratified with an immediate onset of hypolimnetic hypoxia, destratified, and then, with the warm, calm period, restratified and became anoxic until the mooring was removed (Figure 4). In 2018, similar to the pattern at Site 4, the onset of hypoxia was approximately concurrent with the sudden cooling (Figure 3 w; Figure 4), while in 2019 hypoxia did not occur until approximately 10 days after the cooling event (Figure 3 x; Figure 4).

Discussion

Stratification was usually occurring by late May-early June, at all sites, when the moorings were deployed each year (Figure 4), although it was more intermittent at the shallow, nearshore sites and more persistent at the deeper, offshore sites. Sometimes, stratification continued until the moorings were removed, particularly at Site 4, the deepest site.

Hypoxia generally appeared first in the western, nearshore sites, 1, 3, and 5, and showed a general west-east progression in the deeper sites, 2, 4, 7, and 9, most years (Figure 4). Although hypoxia usually occurred earlier in the eastern, nearshore sites, by late July it was typically intermittent, sometimes disappearing even while stratification persisted. In contrast, at sites 2, 4, and 9, the deepest sites, hypoxia was more persistent once it occurred, often progressing to anoxia. Although stratification sometimes occurred for extended periods at Site 8, hypoxia only occurred briefly, suggesting Site 8 may approximate the eastern boundary of the hypoxic region.

The regular occurrence of hypolimnetic anoxia, even at shallower sites where stratification is more intermittent, is of interest as anoxia influences the sediment exchange rate of some important chemicals (Mortimer 1941, Lee et al 1976). In Lake Erie, in particular, sediment phosphorus release has been shown to accelerate only under anoxic conditions (Anderson et al 2021b). The potential magnitude of this release in a season is a function of the duration and spatial extent of anoxia, which were both much less than for hypoxia. Whether this released phosphorus persists in the water column and influences primary production invites further investigation. Under anoxic conditions, the sediments continue to release reduced substances to the overlying water, which can accumulate in the hypolimnion (Muller et al 2012) and potentially drive oxygen consumption once the water mixes with an oxygenated later. These accumulated reduced substances may be important drivers of hypolimnetic oxygen depletion during periods of restratification.

The focus of monitoring programs on the deepest waters of the central basin (> 20 m) has led to estimates of spatial patterns and extent of hypoxia that neglect nearshore and early season hypoxia (Zhou et al., 2013). However, recent modeling results indicate hypoxia forms first in shallower, nearshore areas due to their relatively thin hypolimnion, which experiences more rapid deoxygenation (Bocaniov and Scavia 2016, Rowe et al 2019). Our results support this latter view; each year hypoxia occurred first in the shallower, western sites (1, 3, 5), before expanding eastward along the nearshore and then into the deeper, offshore sites (2, 4, 9). Although Site 1 is separated from the central basin by the Pelee-Lorain ridge, hypoxia occurred there by mid-July every year, and was intermittent through August, similar to observations at Site 3 (Figure 4) and consistent with recent reports of low oxygen in that area (Perello et al 2017). In 2018 and 2019, hypoxia did not occur at the two deepest sites, 4 and 9, until early September, considerably later than the western-most sites. While there was a general west-east progression in hypoxia onset, a similar progression of the onset of stratification was not evident. All sites showed evidence of stratification by the time the moorings were deployed in late May-early June every year. This mismatch in timing of stratification and hypoxia suggests that the rates of oxygen consumption in water and sediment may vary spatially throughout the central basin.

Hypoxia and stratification were intermittent around the edge of the central basin (Sites 3, 5, 7) likely because upwelling and other physical advection events periodically displaced oxygenated water from fully-mixed, shallow areas with deoxygenated water from further offshore, resulting in pronounced short-term variability (Rowe et al 2019, Flood et al 2021, Valipour et al 2021). The offshore sites show a more consistent pattern, usually a progressive deepening of thermocline, though timing and thermocline depth/hypolimnion thickness differs each year, even at Sites 4 and 9, the deepest sites. Interestingly, the sudden pre-destratification cooling event recorded every year (SI Table 3) did not consistently deepen the thermocline at these sites, as might be expected when the epilimnion cools, reducing the surface-bottom density gradient, allowing deeper mixing. In fact, at Sites 4 and 9, the thermocline became shallower following this event in some years, resulting in a thicker hypolimnion (Figure 3 d, e, k), and in some instances hypoxia did not begin until the cooling event occurred (Figure 3 q, w, x). While hypoxia and stratification had become intermittent at most sites by September, they persisted at Site 4, the deepest site, until the moorings were removed.

The rapid restratification that occurred during the warm, calm period in late September 2017 was accompanied by rapid, bottom DO declines that reached hypoxic levels at sites 1, 5, 7, and 9. Jabbari et al (2019) also reported local DO depletion and possible hypoxia in the western basin during this event, indicating the potential for hypoxia to reestablish late in the season. Interestingly, our data suggest the possibility that benthic oxygen production via photosynthesis may have prevented site 8 from experiencing hypoxia during this event (SI Figure 2v), as just prior to the event, DO had been higher at the bottom than at intermediate depths.

Benthic primary production has been previously reported in Lake Erie's central basin (Burns et al 2005) and intriguingly, our measurements reveal diurnal DO fluctuations throughout the water column at most monitoring sites, indicating daytime photosynthesis even at deep, bottom sensors experiencing hypoxia (e.g. Figure SI 3 v, w, x). Both meroplanktonic diatoms (Carrick et al 2005, Lashaway and Carrick 2010) and picocyanobacteria (Wilhelm et al 2006) have been documented below the thermocline in the central basin and may be contributing to these observed DO patterns.

Excessive primary production is generally regarded as the main driver of hypoxia as settled, decaying organic matter provides the oxygen demand that depletes hypolimnetic oxygen (Diaz 2001). In Lake Erie central basin hypoxia has generally been regarded as a consequence of western basin algal blooms, which occur in the summer and produce large amounts of organic matter that is carried eastward, eventually settling in the central basin. However, our results highlight the fact that these two phenomena are spatially and temporally distinct. In the deeper areas of the central basin hypoxia occurs mainly from late August through September, roughly temporally concurrent with western basin algal blooms, but spatially separated by upwards of 200 km (Figure 1). Furthermore, the hypoxia we documented in the western central basin began as early as July, before western basin algal blooms typically occur. Accumulating evidence suggests that winter productivity may be an important organic matter source driving hypoxia (Willhelm et al 2014), including winter-spring diatom production (Reavie et al 2016). Concurrently, the role of primary production in the central basin remains unclear. Further quantification of the relative contributions of organic matter from various sources will inform modeling efforts and better clarify expectations regarding the response of hypoxia to future phosphorus loading changes. If sediment oxygen demand includes a significant legacy component (Del Giudice et al 2018) that integrates the influence of excessive productivity over both space and time it is likely to obfuscate a response to any realized phosphorus input reductions.

To document future changes in hypoxia, appropriate measurement of the spatial and temporal extent will be critical. The US EPA Great Lakes National Program Office maintains a network of 10 sites in Lake Erie’s central basin (Figure 1) that are monitored approximately every three weeks from June through September to assess hypoxia dynamics (U.S. EPA 2021). Data from this network have been an important basis for estimating hypoxic area (Zhou et al. 2013). Our results indicate that hypoxia is more spatially, and perhaps temporally, extensive than the coverage of this network, forming first in the shallower nearshore areas along the southern shore before extending into the deeper, offshore region and persisting into October in some years. The shallower sites along the Ohio shore demonstrated changes in stratification and hypoxia on a temporal scale of days to weeks. Accurate estimation of indicators, such as hypoxic area, hypoxic volume, or average bottom DO concentration, chosen as metrics to assess the response of hypoxia to phosphorus load changes invites expanded monitoring to better capture the spatial and temporal characteristics revealed by our data. While our mooring data capture early-season hypoxia formation in shallower areas west of the central basin and suggest that hypoxia expands from the west to the east, observations from the shallower areas in the eastern central basin are limited. Thus, to better document hypoxic extent, an expanded network should include eastern central basin moorings located in the 10-15 m depth range. Xu et al (2021) reached a similar conclusion, pointing out that limited monitoring in nearshore areas around the hypoxic zone periphery limits the accuracy of hypoxia spatial extent estimation. While autonomous vehicles such as buoyancy gliders could potentially complement moorings in the central basin, performing those missions at shallower depths is difficult. In addition to direct observation of dissolved oxygen, monitoring of biological indicators such as benthic fauna can be a useful time-integrated indicator of the occurrence and severity of hypoxia (Reynoldson et al 1993; Karatayev et al 2018).

Our results indicate that the response of hypoxia to productivity tempered by decreasing phosphorus loads may be difficult to accurately assess. In addition to possible time-lags, differing annual weather conditions influence hypoxia extent and duration. Setting expectations accordingly will be critical in the adaptive management process.

References

Anderson, H. S., T. H. Johengen, C. M. Godwin, H. Purcell, P. J. Alsip, S. A. Ruberg, and L. A. Mason. 2021a. Continuous *In Situ* Nutrient Analyzers Pinpoint the Onset and Rate of Internal P Loading under Anoxia in Lake Erie's Central Basin. ACS EST Water. 1 (4), 774-781. doi.org/10.1021/acsestwater.0c00138.

Anderson, H. S., T. H. Johengen, R. Miller, and C. M. Godwin. 2021b. Accelerated sediment phosphorus release in Lake Erie's central basin during seasonal hypoxia. Limnology and Oceanography, 66: 3582-3595. doi: 10.1002/lno.11900.

Annex 4, Great Lakes Water Quality Agreement (GLWQA) Objectives and Targets Task Team. 2015. Recommended Phosphorus Load Targets for Lake Erie. Final Report to the Nutrients Annex Subcommittee. Available online. https://www.epa.gov/sites/default/files/2015-06/documents/report-recommended-phosphorus-loading-targets-lake-erie-201505.pdf

Beeton, A. M. 1961. Environmental changes in Lake Erie. Transactions of the American Fisheries Society, 90: 153-159. doi: 10.1577/1548-8659(1961)90[153:ECILE]2.0.CO;2.

Beeton, A. M. 1965. Eutrophication of the St. Lawrence Great Lakes. Limnology and Oceanography. 10: 240-254. doi: 10.4319/lo.1965.10.2.0240.

Bocaniov, S. A., and D. Scavia. 2016. Temporal and spatial dynamics of large lake hypoxia: Integrating statistical and three-dimensional dynamic models to enhance lake management criteria. Water Resources Research. 52: 4247-4263. doi: 10.1002/2015WR018170.

Bocaniov, S. A., K. G. Lamb, W. T. Liu, Y. R. Rao, and R. E. H. Smith. 2020. High Sensitivity of Lake Hypoxia to Air Temperatures, Winds, and Nutrient Loading: Insights From a 3-D Lake Model. Water Resources Research. 56: Article Number: e2019WR027040. doi: 10.1029/2019WR027040.

Britt, N. W. 1955. Stratification in western Lake Erie in summer of 1953: Effects on the Hexagenia (Ephemeroptera) population. Ecology. 36: 239-244. doi: 10.2307/1933229

Britt, N. W., E. J. Skoch, and K. R. Smith. 1968. Record low dissolved oxygen in the island area of Lake Erie. The Ohio Journal of Science. 68: 175-179.

Burns, N. M., D. C. Rockwell, P. E. Bertram, D. M. Dolan, and J. J. H. Ciborowski. 2005. Trends in temperature, Secchi depth, and dissolved oxygen depletion rates in the central basin of Lake Erie, 1983-2002. Journal of Great Lakes Research. 31, supplement 2: 35-49. doi: 10.1016/S0380-1330(05)70303-8.

Carpenter, S. R., N. F. Caraco, NF , D. L. Correll, R. W. Howarth, A. N. Sharpley, and V. H. Smith. 1998. Nonpoint pollution of surface waters with phosphorus and nitrogen. Ecological Applications. 8: 559-568. doi: 10.2307/2641247.

Carr, J. F. 1962. Dissolved oxygen in Lake Erie, past and present. Great Lakes Research Division. University of Michigan, Publication no. 9, 2-14.

Carr, J. F., V. C. Applegate, and M. Keller. 1965. A recent occurrence of thermal stratification and low dissolved oxygen in western Lake Erie. The Ohio Journal of Science. 65: 319-327.

Carrick, H. J., J. B. Moon, and B. F. Gaylord. 2005. Phytoplankton dynamics and hypoxia in Lake Erie: A hypothesis concerning benthic-pelagic coupling in the central basin. Journal of Great Lakes Research. 31 (Supplement 2): 111-124. doi: 10.1016/S0380-1330(05)70308-7.

Del Giudice, D., Y. Zhou, E. Sinha, and A. M. Michalak. 2018. Long-term phosphorus loading and springtime temperatures explain interannual variability of hypoxia in a large temperate lake. Environmental Science & Technology. 52: 2046-2054. doi: 10.1021/acs.est.7b04730.

Delorme, L. D. 1982. Lake Erie oxygen; The prehistoric record. Canadian Journal of Fisheries and Aquatic Sciences. 39: 1021-1029. doi: 10.1139/f82-137.

DePinto, J. V., T. C. Young, and L. M. Mcilroy. 1986. Great Lakes water quality improvement – The strategy of phosphorus discharge control is evaluated. Environmental Science & Technology. 20: 752-759. doi: 10.1021/es00150a001.

Diaz, R. J. Overview of hypoxia around the world. 2001. Journal of Environmental Quality. 30: 275-281.doi: 10.2134/jeq2001.302275x

Fish, C. J. and Associates. 1960. Limnological survey of eastern and central Lake Erie, 1928-1929. US Fish and Wildlife Service. Special Scientific Report – Fisheries no. 334.

Flood, B., M. Wells, J. D. Midwood, J. Brooks, Y. L. Kuai, and J. Z. Li. 2021. Intense variability of dissolved oxygen and temperature in the internal swash zone of Hamilton Harbour, Lake Ontario. Inland Waters. doi: 10.1080/20442041.2020.1843930.

Great Lakes Water Quality Agreement. 2012. Protocol amending the agreement between Canada and the United States of America on Great Lakes Water Quality, signed September 7, 2012. https://binational.net/glwqa-aqegl/

Jabbari, A., J. D. Ackerman, L. Boegman, and Y. Zhao. 2019. Episodic hypoxia in the western basin of Lake Erie. Limnology and Oceanography. 64: 2220-2236. doi: 10.1002/lno.11180.

Jane, S. F., G. J. A. Hansen, B. M. Kraemer, P. R. Leavitt, J. L. Mincer, R. L. North, R. M. Pilla, J. T. Stetler, C. E. Williamson, R. I. Woolway, L. Arvola, S. Chandra, C. L. DeGasperi, L. Diemer, J. Dunalska, O. Erina, G. Flaim, H. P. Grossart, K. D. Hambright, C. Hein, J. Hejzlar, L. L. Janus, J. P. Jenny, J. R. Jones, L. B. Knoll, B. Leoni, E. Mackay, S. I. S. Matsuzaki, C. McBride, D. C. Muller-Navarra, A. M. Paterson, D. Pierson, M. Rogora, J. A. Rusak, S. Sadro, E. Saulnier-Talbot, M. Schmid, R. Sommaruga, W. Thiery, P. Verburg, K. C. Weathers, G. A. Weyhenmeyer, K. Yokota, and K. C. Rose. 2021. Widespread deoxygenation of temperate lakes. Nature. 594: 66-+. doi: 10.1038/s41586-021-03550-y.

Jenny, J. P., P. Francus, A. Normandeau, F. Lapointe, M. E. Perga, A. Ojala, A. Schimmelmann, and B. Zolitschka. 2016. Global spread of hypoxia in freshwater ecosystems during the last three centuries Is caused by rising local human pressure. Global Change Biology. 22: 1481-1489. doi: 101111/gcb.13193.

Karatayev, A.Y., L. E. Burlakova, K. Mehler, S. A. Bocaniov, P. D. Collingsworth, G. Warren, R. T. Kraus, and E. K. Hinchey. 2018. Biomonitoring using invasive species in a large lake: Dreissena distribution maps hypoxic zones. Journal of Great Lakes Research. 44: 639-649. doi: 10.1016/j.jglr.2017.08.001.

Kraus, R. T., C. T. Knight, T. M. Farmer, A. M. Gorman, P. D. Collingsworth, G. L. Warren, P. M. Kocovsky, and J. D. Conroy. 2015. Dynamic hypoxic zones in Lake Erie compress fish habitat, altering vulnerability to fishing gears. Canadian Journal of Fisheries and Aquatic Sciences. 72: 797-806. doi: 10.1139/cjfas-2014-0517.

Lashaway, A. R., and H. J. Carrick. 2010. Effect of light, temperature and habitat quality on meroplanktonic diatom rejuvenation in Lake Erie: implications for seasonal hypoxia. Journal of Plankton Research. 32: 479-490. doi: 10.1093/plankt/fbp147.

Lee, G. F., W. C. Sonzogni, and R. D. Spear. 1976. Significance of oxic vs. anoxic conditions for Lake Mendota sediment phosphorus release. Pages 363–369 *in* Golterman (ed.), Interactions between sediments and freshwater. Junk and Pudoc.

Makarewicz, J. C., and P. Bertram. 1991. Evidence for the restoration of the Lake Erie ecosystem- water quality, oxygen levels, and pelagic function appear to be improving. BioScience. 41: 216-223. doi: 10.2307/1311411.

Makarewicz, J. C., and P. Bertram. 1993. Special issue of the Journal of Great Lakes Research – evidence for the restoration of the Lake Erie ecosystem. Journal of Great Lakes Research. 19: 197-197. doi: 10.1016/S0380-1330(93)71209-5.

Michalak, A. M., E. J. Anderson, D. Beletsky, S. Boland, N. S. Bosch, T. B. Bridgeman, J. D. Chaffin, K. Cho, R. Confesor, I. Daloglu, J. V. DePinto, M. A. Evans, G. L. Fahnenstiel, L. L. He, J. C. Ho, L. Jenkins, T. H. Johengen, K. C. Kuo, E. LaPorte, X. J. Liu, M. R. McWilliams, M. R. Moore, D. J. Posselt, R. P. Richards, D. Scavia, A. L. Steiner, E. Verhamme, D. M. Wright, and M. A. Zagorski. 2013. Record-setting algal bloom in Lake Erie caused by agricultural and meteorological trends consistent with expected future conditions. Proceedings of the National Academy of Sciences of the United States of America. 110: 6448-6452. doi: 10.1073/pnas.1216006110.

Mortimer, C. H. 1941. The exchange of dissolved substances between mud and water in lakes. Journal of Ecology. 29: 280–329.

Muller, B., L. D. Bryant, A. Matzinger, and A. Wuest. 2012. Hypolimnetic oxygen depletion in eutrophic lakes. Environmental Science & Technology. 46: 9964-9971. doi: 10.1021/es301422r

Perello, M. M., D. D. Kane, P. Golnick, M. C. Hughes, M. A. Thomas, and J. D. Conroy. 2017. Effects of local weather variation on water-column stratification and hypoxia in the Western, Sandusky, and Central Basins of Lake Erie. Water. 9: 279. doi: 10.3390/w9040279.

Powers, C. F., D. L. Jones, P. C. Mundinger, and J. C. Ayers. 1959. Exploration of collateral data potentially applicable to Great Lakes hydrography and fisheries. Great Lakes Research Institute. The University of Michigan. Ann Arbor, MI.

Powers, C. F., D. L. Jones, P. C. Mundinger, and J. C. Ayers. 1960. Application of data collected along shore to conditions in Lake Erie. Great Lakes Research Division. University of Michigan, Publication no. 4, 64-78.

Reavie, E. D., M. J. Cai, M. R. Twiss, H. J. Carrick, T. W. Davis, T. H. Johengen, D. Gossiaux, D. E. Smith, D. Palladino, A. Burtner, and G. V. Sgro. 2016. Winter-spring diatom production in Lake Erie is an important driver of summer hypoxia. Journal of Great Lakes Research. 42: 608-618. doi: 10.1016/j.jglr.2016.02.013.

Reynoldson, T. B. and A. L. Hamilton. 1993. Historic changes in populations of burrowing mayflies (Hexagenia limbata) from Lake Erie based on sediment tusk profiles. Journal of Great Lakes Research, 19: 250-257. doi: 10.1016/S0380-1330(93)71215-0.

Rowe, M. D., E. J. Anderson, D. Beletsky, C. A. Stow, S. D. Moegling, J. D. Chaffin, J. C. May, P. D. Collingsworth, A. Jabbari, J. D. Ackerman. 2019. Coastal upwelling influences hypoxia spatial patterns and nearshore dynamics in Lake Erie. Journal of Geophysical Research-Oceans. 124: 6154-6175. doi.org/10.1029/2019JC015192.

Rowland, F. E., C. A. Stow, L. T. Johnson, and R. M. Hirsch. 2021. Lake Erie tributary nutrient trend evaluation: normalizing concentrations and loads to reduce flow variability. Ecological Indicators. 125: 107601. doi.org/10.1016/j.ecolind.2021.107601

Ruberg, S. A., E. Guasp, N. Hawley, R. W. Muzzi, S. B. Brandt, H. A. Vanderploeg, J. C. Lane, T. Miller, and S. A. Constant. 2008. Societal Benefits of the Real-Time Coastal Observation Network (ReCON): Implications for Municipal Drinking Water Quality. Marine Technology Society Journal. 42: 103-109. doi: 10.4031/002533208786842471.

Scavia, D., J. D. Allan, K. K. Arend, S. Bartell, D. Beletsky, N. S. Bosch, S. B. Brandt, R. D. Briland, I. Daloglu, J. V. DePinto, D. M. Dolan, M. A. Evans, T. M. Farmer, D. Goto, H. J. Han, T. O. Hook, R. Knight, S. A. Ludsin, D. Mason, A. M. Michalak, R. P. Richards, J. J. Roberts, D. K. Rucinski, E. Rutherford, D. J. Schwab, T. M. Sesterhenn, H. Y. Zhang, and Y. T. Zhou. 2014. Assessing and addressing the re-eutrophication of Lake Erie: Central basin hypoxia. Journal of Great Lakes Research. 40: 226-246. doi: 10.1016/j.jglr.2014.02.004.

Schmidt, W. 1928. Über Die Temperatur- Und Stabili-Tätsverhältnisse Von Seen, Geografiska Annaler, 10:1-2, 145-177. doi: 10.1080/20014422.1928.11880475.

Simpson, J. H. and D. Bowers. 1981. Models of stratification and frontal movement in shelf seas. Deep Sea Research Part A. Oceanographic Research Papers. 28: 727-738. doi: 10.1016/0198-0149(81)90132-1.

Simpson, J. H. and D. G. Bowers. 1984. The role of tidal stirring in controlling the seasonal heat cycle in shelf seas. Annales Geophysicae 2(4): 411-416.

Simpson, J. H., D. G. Hughes, and N. C. G. Morris. 1977. The relation of seasonal stratification to tidal mixing on the continental shelf. In: A voyage of discovery, M. Angel, editor, Deep-Sea Research (supplement), pp. 327-340.

Stow, C. A., K. Glassner-Shwayder, D. Lee, L. Wang, G. Arhonditsis, J. V. DePinto, and M.R. Twiss. 2020. Lake Erie phosphorus targets: An imperative for active adaptive management. Journal of Great Lakes Research. 46: 672-676. doi: 10.1016/j.jglr.2020.02.005

U.S. EPA 2021. Lake Erie Dissolved Oxygen Monitoring Program Technical Report: Dissolved Oxygen and Temperature Profiles for the Open Waters of the Central Basin of Lake Erie during Summer/Fall of 2016. (EPA 950-R-21-004).

Valipour, R., L.F. Leon, T. Howell, A. Dove, and Y. R. Rao. 2021. Episodic nearshore-offshore exchanges of hypoxic waters along the north shore of Lake Erie. Journal of Great Lakes Research. 47: 419-436. doi: 10.1016/j.jglr.2021.01.014

Vanderploeg, H. A., S. A. Ludsin, S. A. Ruberg, T. O. Hook, S. A. Pothoven, S. B. Brandt, G. A. Lang, J. R. Liebig, and J. F. Cavaletto. 2009. Hypoxia affects spatial distributions and overlap of pelagic fish, zooplankton, and phytoplankton in Lake Erie. Journal of Experimental Marine Biology and Ecology. 381, Supplement 1: S92-S107. doi: 10.1016/j.jembe.2009.07.027.

Watson, S. B., C. Miller, G. Arhonditsis, G. L. Boyer, W. Carmichael, M. N. Charlton, R. Confesor, D. C. Depew, T. O. Hook, S. A. Ludsin, G. Matisoff, S. P. McElmurry, M. W. Murray, R. P. Richards, Y. R, Rao, M. M. Steffen, and S. W. Wilhelm. 2016. The re-eutrophication of Lake Erie: Harmful algal blooms and hypoxia. Harmful Algae. 56: 44-66. doi: 10.1016/j.hal.2016.04.010.

Wilhelm, S. W., G. R. LeClair, G. S. Bullerjahn, R. M. McKay, M. A. Saxton, M. R. Twiss, and R. A. Bourbonniere. 2014. Seasonal changes in microbial community structure and activity imply winter production is linked to summer hypoxia in a large lake. FEMS Microbiology Ecology. 87: 475-485. Doi: 10.1111/1574-6941.12238.

Wilhelm, S. W., G. S. Bullerjahn, M. L. Eldridge, J. M. Rinta-Kanto, L. Poorvin, and R. A. Bourbonniere. 2006. Seasonal hypoxia and the genetic diversity of prokaryote populations in the central basin hypolimnion of Lake Erie: Evidence for abundant cyanobacteria and photosynthesis. Journal of Great Lakes Research. 32: 657-671. doi: 10.3394/0380-1330(2006)32[657:SHATGD]2.0.CO;2.

Xu, W., P. D. Collingsworth, R. Kraus, and B. Minsker. 2021. Spatio-temporal analysis of hypoxia in the central basin of Lake Erie of North America. Water Resources Research. 57, e2020WR027676. doi.org/10.1029/2020WR027676.

Zhou, Y. T., A. M. Michalak, D. Beletsky, Y. R. Rao, and R. P. Richards. 2015. Record-Breaking Lake Erie hypoxia during 2012 drought. Environmental Science & Technology. 49: 800-807. doi: 10.1021/es503981n.

Zhou, Y., D. R. Obenour, D. Scavia, T. H. Johengen, and A. M. Michalak. 2013. Spatial and temporal trends in Lake Erie Hypoxia, 1987-2007. Environmental Science & Technology. 47: 899-905. doi: 10.1021/es303401b.

Acknowledgements

We thank Russ Miller and captains of the NOAA R4108, R5501, and R5503 vessels for their assistance deploying and retrieving the moorings. This work was supported by the National Oceanic and Atmospheric Administration's National Centers for Coastal Ocean Science Competitive Research Program under Grant NA16NOS4780209 to the University of Michigan and through the NOAA Cooperative Agreement with the Cooperative Institute for Great Lakes Research (CIGLR) at the University of Michigan (NA17OAR4320152). This is CIGLR contribution XXXX, CHRP contribution XXX, and NOAA-GLERL contribution XXXX. Any use of trade, product, or firm names is for descriptive purposes only and does not imply endorsement by the US Government.

Table Captions

Table 1

Hypolimnetic hypoxia and anoxia metrics based on bottom-most DO sensor at each mooring location.

[*]The deepest DO sensor at Site 2 in 2017 was at 17 m, approximately 3 m off the bottom. Metrics for hypoxia and anoxia may be underestimates.

[**]The deepest DO sensor at Site 7 in 2018 was at 19.6 m but was excluded from analyses due to poor data quality. In its place, we describe the hypoxia and anoxia metrics for the second sensor off the bottom at 17.1 m. Metrics for hypoxia and anoxia are likely underestimates.

[***]Site 8 experienced brief hypoxia at 11 m, which is not the deepest sensor and therefore not described in this table.

[****]The deepest DO sensor at Site 7 in 2019 was at 14.1 m, almost 6 m off the bottom. Metrics for hypoxia and anoxia are almost certainly underestimates.

[1]Bottom sensor was hypoxic when the mooring was retrieved.

[2]Bottom sensor indicated DO was dropping rapidly with the 2017 restratification and was almost hypoxic when the mooring was retrieved.

[3]Bottom sensor was anoxic when the mooring was retrieved.

[4]Bottom sensor had become normoxic but returned rapidly to anoxia with the 2017 restratification and was anoxic when the mooring was retrieved.

Year	**Table 1**	Site 1	Site 2	Site 3	Site 4	Site 5	Site 7	Site 8	Site 9
	Water depth (m)	12	20	15.25	24.25	15.25	20	13.75	21
2017	Deployment	5/22 - 9/25	6/9 - 10/3	5/23 - 9/27	5/23 - 9/27	5/23 - 10/2	5/23 - 9/27	5/23 - 9/26	5/24 - 9/26
	Bottom DO sensor depth (m)	11.7	17*	14.9	23.8	14.8	19.6	13.5	20.4
	Hypoxic events	10	20	16	6	32	9	0	27
	Hypoxic days	21[1]	17	39[2]	55[3]	40	31[3]	0	30[4]
	Hypoxia first appearance	July 7	July 14	June 18	August 2	July 11	August 6	-	July 28
	Longest hypoxia onset	July 14	August 31	July 13	August 9	July 15	August 13	-	August 5
	Longest hypoxia (d)	11	7	15	50	14	16	0	12
	Anoxic events	5	7	10	1	17	8	0	7
	Anoxic days	4	8	7	37[3]	12	14[3]	0	8[4]
	Anoxia first appearance	July 28	July 25	14-July 14	August 21	July 16	August 25	-	August 28
	Longest anoxia onset	August 19	September 1	August 15	August 21	August 14	September 16	-	September 22
	Longest anoxia (d)	2	6	3	37	4	7	0	5
2018	Deployment	5/22 - 10/10	6/12 - 10/10	5/30 - 10/3	5/30 - 10/3		5/30 - 10/3	5/23 - 10/25	5/23 - 10/25
	Bottom DO sensor depth (m)	11.7	19.5	14.9	23.8	LOST	17.1**	13.5***	20.4
	Hypoxic events	20	9	11	1	-	12	0	2
	Hypoxic days	31	37	50	26[3]	-	18	0	31
	Hypoxia first appearance	July 15	July 31	July 4	September 7	-	August 9	-	September 10
	Longest hypoxia onset	August 6	August 7	August 25	September 7	-	August 30	-	September 11
	Longest hypoxia (d)	13	29	17	26	-	9	0	30
	Anoxic events	9	4	8	4	-	0	0	2
	Anoxic days	15	7	17	23[3]	-	0	0	8
	Anoxia first appearance	August 7	August 22	July 17	September 9	-	-	-	October 3
	Longest anoxia onset	August 12	September 7	August 11	September 12	-	-	-	October 4
	Longest anoxia (d)	6	3	8	9	-	0	0	7
2019	Deployment	5/21 - 10/7	5/21 - 10/10	5/21 - 10/8	5/21 - 10/10	5/29 - 10/8	5/30 - 10/9	5/29 - 10/8	5/30 - 10/8
	Bottom DO sensor depth (m)	11.7	19.5	14.9	23.8	14.8	14.1****	13.5	20.4
	Hypoxic events	14	6	26	5	15	18	4	6
	Hypoxic days	40	67	51	43	40	9	2	33
	Hypoxia first appearance	July 4	July 16	July 3	August 19	July 31	August 27	August 24	August 29
	Longest hypoxia onset	July 8	August 4	August 19	August 28	August 12	September 11	September 13	September 4
	Longest hypoxia (d)	15	61	16	42	18	2	1	31
	Anoxic events	29	6	20	2	17	8	0	5
	Anoxic days	12	44	27	27	23	2	0	20
	Anoxia first appearance	July 13	August 23	August 14	September 11	August 16	September 11	-	September 13
	Onset longest anoxia	July 13	August 31	September 8	September 14	September 8	September 29	-	September 14
	Longest anoxia (d)	3	34	5	26	5	1	0	9

Figure Captions

Figure 1

Lake Erie map depicting mooring locations. Black triangles denote US EPA hypoxia monitoring sites.

Figure 2

Interpolated nearshore mooring sites' observations for temperature (top) and DO (bottom). Black, horizontal, dashed lines indicate sensor depths on each mooring. The band across the top of each temperature panel depicts satellite-measured surface temperature data at that location. The band across the top of each DO panel indicates freshwater saturation DO concentration at the satellite-measured temperature. The vertical scale on each panel is from 0-15 m to keep the resolution consistent; brown band indicates lake bottom at that site. A white contour line indicates the upper hypoxia extent (DO < 2 mg/L) in each dissolved oxygen panel. Note that the upper extent of hypoxia may not be well-determined at sites 3 and 5 due to low DO resolution near the bottom.

Figure 3

Interpolated offshore mooring sites' observations for temperature (top) and DO (bottom). Black, horizontal, dashed lines indicate sensor depths on each mooring. The band across the top of each temperature panel depicts satellite-measured surface temperature data at that location. The band across the top of each DO panel indicates freshwater saturation DO concentration at the satellite-measured temperature. The vertical scale on each panel is from 0-24 m to keep the resolution consistent; brown band indicates lake bottom at that site. A white contour line indicates the upper hypoxia extent (DO < 2 mg/L) in each dissolved oxygen panel.

Figure 4

Sitewise depiction of stratification and bottom hypoxia and anoxia for each site and year. The deployment period for each mooring is depicted by the gray line and endcaps. The duration of stratification (1ºC difference in daily mean temp from surface to bottom) is shown as a thick black line. Daily mean hypoxia (dissolved oxygen <2 mg/L) is shown in blue and daily mean anoxia (dissolved oxygen <0.15 mg/L) is shown in red. [1] The bottom DO sensor in 2017 at site 2 was at 17 m, but at 19.5 m in 2018 and 2019. [2] The bottom DO sensor in 2019 at site 7 was at 16 m. The inset gray and black line depicts the strength of stratification (higher PEA is a thicker line), with discrete thresholds denoted in the legend.

Figure 1

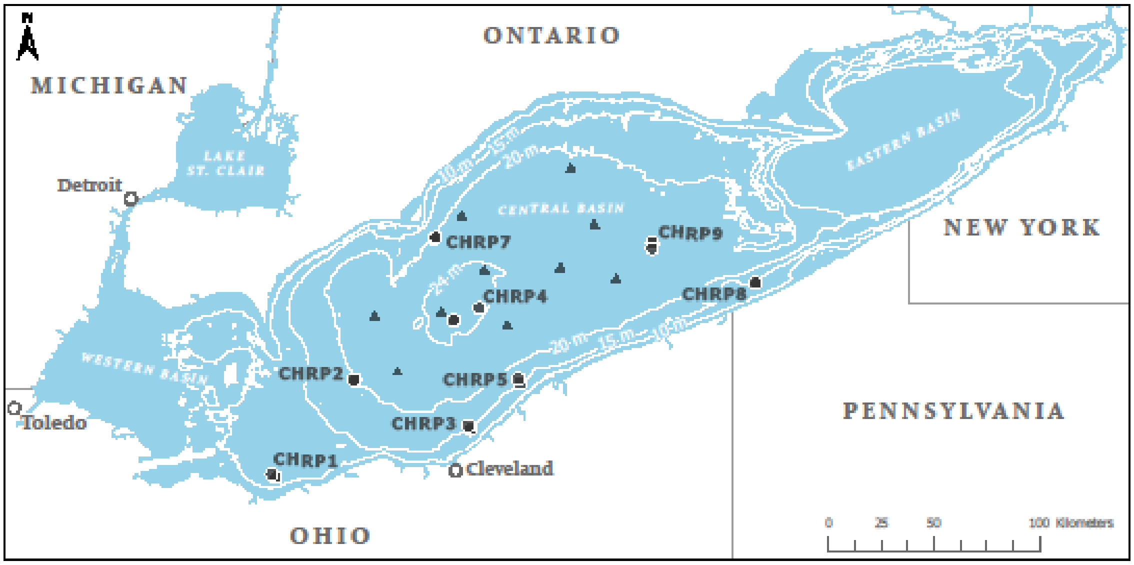

ONTARIO
MICHIGAN
LAKE ST. CLAIR
Detroit
CENTRAL BASIN
EASTERN BASIN
NEW YORK
CHRP7
CHRP9
CHRP4
CHRP8
WESTERN BASIN
CHRP2
CHRP5
CHRP3
CHRP1
Toledo
Cleveland
PENNSYLVANIA
OHIO
10 m
15 m
20 m
24 m
0 25 50 100 Kilometers

Figure 2

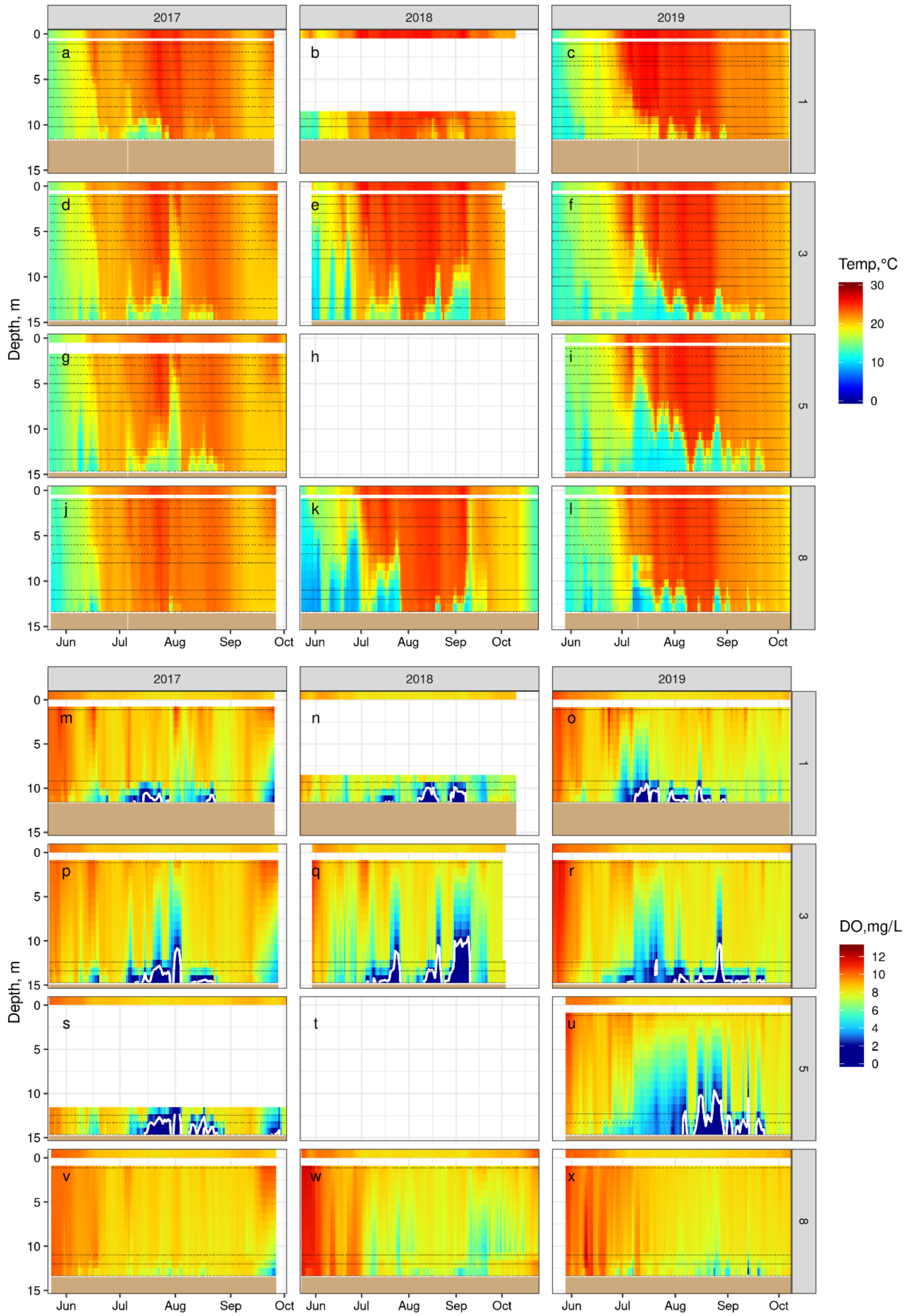
2017
2018
2019
a
b
c
d
e
f
g
h
i
j
k
l
1
3
5
8
Depth, m
0
5
10
15
Temp,°C
30
20
10
0
Jun
Jul
Aug
Sep
Oct
m
n
o
p
q
r
s
t
u
v
w
x
DO,mg/L
12
10
8
6
4
2
0

Figure 3

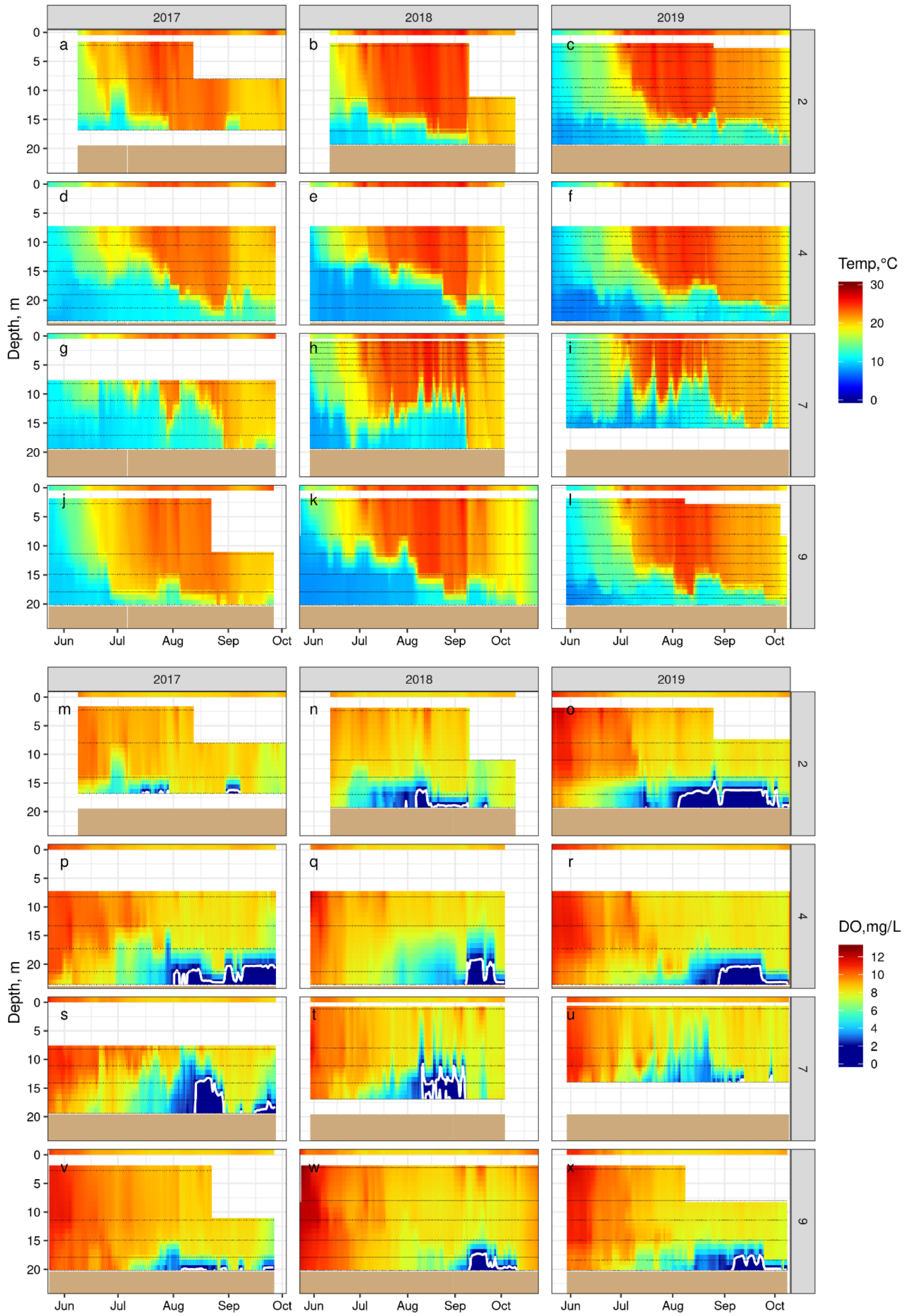

2017
2018
2019
Depth, m
Temp,°C
30
20
10
0
DO,mg/L
12
10
8
6
4
2
0
Jun
Jul
Aug
Sep
Oct

Figure 4

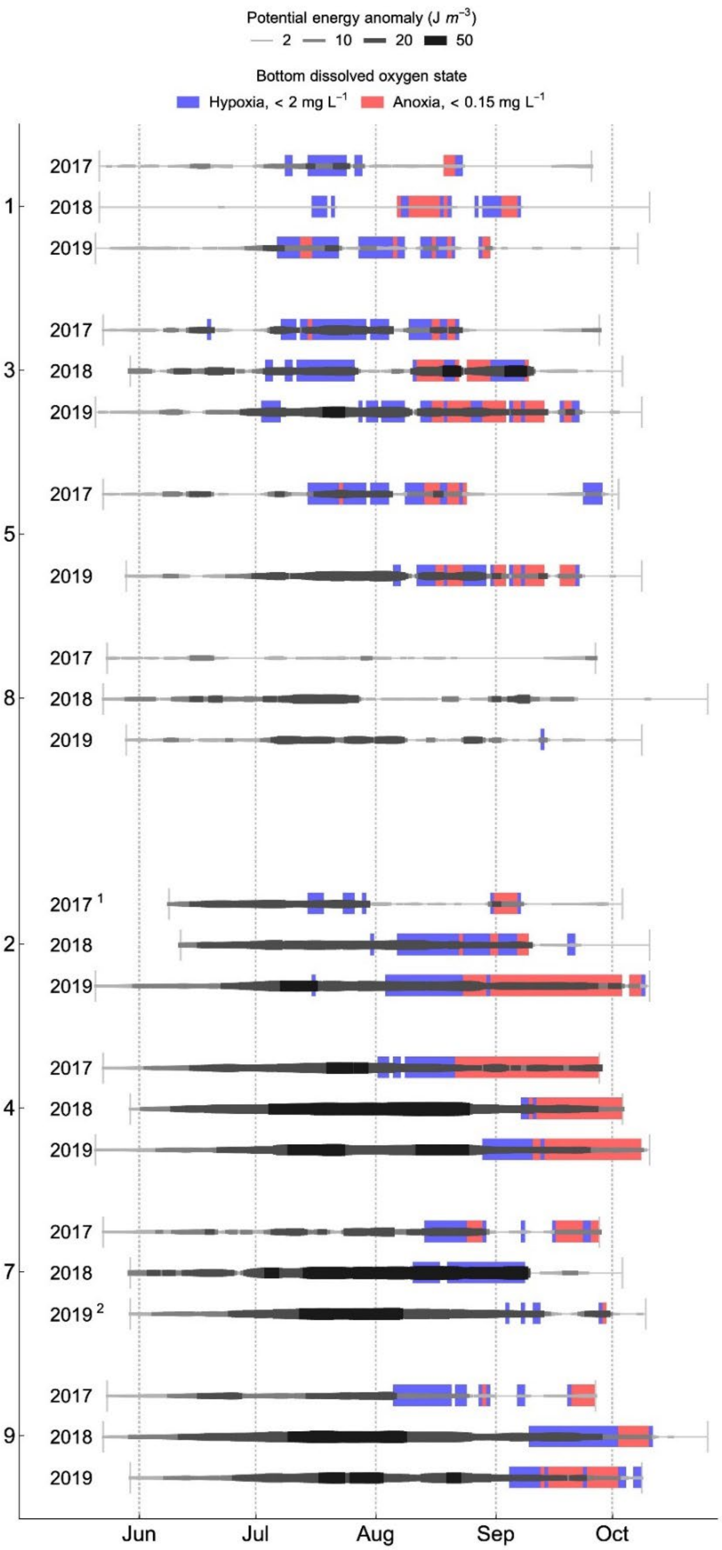

Potential energy anomaly (J m^{-3})
2
10
20
50
Bottom dissolved oxygen state
Hypoxia, < 2 mg L^{-1}
Anoxia, < 0.15 mg L^{-1}
1
2017
2018
2019
3
2017
2018
2019
5
2017
2019
8
2017
2018
2019
2
2017 1
2018
2019
4
2017
2018
2019
7
2017
2018
2019 2
9
2017
2018
2019
Jun
Jul
Aug
Sep
Oct